



Research article

The impact of tube bundle layout on the thermal and fluidic behaviour of liquid lead–bismuth eutectic in a helical-coiled once-through steam generator

Mashrur Muntasir Nuhash, Md. Rezwanul Karim, Arafat A. Bhuiyan*

Department of Mechanical and Production Engineering (MPE), Islamic University of Technology (IUT), Board Bazar, Gazipur, 1704, Bangladesh

ARTICLE INFO

Keywords:

Liquid metal
Lead-bismuth eutectic
Heat transfer
Computational fluid dynamics
Helically-coiled once through steam generator

ABSTRACT

This study introduces a numerical model to assess the thermal and frictional properties of LBE crossflow over tube bundles on the shell side of a Helical-coiled Once-Through Steam Generator (H-OTSG) considering different arrangements, including inline, obliquely staggered, triangular, and rotated square configurations. The $k-\omega$ SST turbulence model combined with Kays turbulent Prandtl number model is utilized to develop the numerical model. The simulation results have been validated against experimental data and empirical correlations. The layouts of the tube bundles significantly influence the generation of transverse flow, vortical structures and rate of heat transfer in the flow domain. The maximum Nusselt number of 8.2 is observed for the triangular layout as significant crossflow is induced, which is a 10% increase compared to the inline arrangement where the Nusselt number is 7.45. Triangle layouts also exhibit a higher friction factor of 0.45, marking a 20% increase compared to the 0.45 friction factor observed in the inline arrangement. Increasing the oblique angle usually reduces the heat transfer rate and friction factor. Yet, at a 45-degree layout, higher turbulence intensity results in a Nu of 7.05, surpassing 6.93 observed at 30° but falling short of 7.15 at 15°. Nu decreases for rotated square arrangements, but a friction factor greater than the inline arrangement is observed at higher diagonal pitches. The Thermal Enhancement Factor (THEF) is employed to assess the thermal effectiveness of the different tube bundle layouts, and the maximum THEF of 1.1 is observed for the layout with an oblique angle of 45°. Favorable THEF values of 1.06 and 1.05 are recorded for the triangular layout and 30-degree oblique angle, respectively. This numerical study will assist the design and development of LBE H-OTSG.

1. Introduction

Nuclear energy stands out as a dependable source for efficient electricity generation and clean energy production. Ongoing research is concentrated on enhancing reactor design, improving coolant performance, ensuring thermal stability, and augmenting corrosion and radiation resistance of materials, especially composite materials used in reactors [1]. The cooling process of nuclear reactors is intricately tied to the coolant's properties and its performance in natural, mixed, and forced convection, in addition to the design of the heat exchanger [2]. Similar to metals, metal alloys and complex transitional metal oxides, liquid metals show excellent electrical and

* Corresponding author.

E-mail address: arafat@iut-dhaka.edu (A.A. Bhuiyan).

<https://doi.org/10.1016/j.heliyon.2024.e24149>

Received 30 August 2023; Received in revised form 1 December 2023; Accepted 4 January 2024

Available online 7 January 2024

2405-8440/© 2024 Published by Elsevier Ltd.

This is an open access article under the CC BY-NC-ND license

(<http://creativecommons.org/licenses/by-nc-nd/4.0/>).

thermal conductivity due to their electron-rich metallic cores, demonstrating their prospect as effective coolants [3]. Besides the outstanding heat transfer characteristics, their suitable thermo-physical properties and exceptional neutronic attributes have enabled liquid metals to gain significant interest for their potential application as coolants in nuclear reactors [4]. Subsequently, the application of liquid metals such as Sodium (Na), lead (Pb), and lead-bismuth eutectic alloy (LBE) have been extensively studied in Generation-IV Fast Breeder Reactors (GEN-IV FBR), among which lead-based reactors are deemed promising due to its chemical inertness [5]. To achieve further improvements in both the performance and compactness of a reactor, the integration of a Helically-coiled Once Through Steam Generator (H-OTSG) is broadly employed, where the flow of liquid metal occurs in the shell side to initiate thermal transport from the primary to the secondary side [6,7].

The design and performance of a heat exchanger are significantly influenced by the properties of the working fluids. Transfer of heat is optimally achieved when the working fluid exhibits high thermal conductivity, a critical characteristic of the cooling process [8]. Liquid metals such as LBE present exceptional thermal properties such as remarkably elevated thermal conductivity and very low Prandtl number (Pr) in the magnitude of 10^{-2} , making them inherently different from conventional fluids [9]. Due to its exceptionally low Pr, the thermal diffusion is dominated by molecular conduction and the thermal boundary layer contains a substantially larger region than conventional fluids [10]. Hence, the flow behaviour of liquid metals differs significantly from that of conventional fluids, necessitating comprehensive research to comprehend their unique characteristics.

So far, to the best of the author's knowledge, no relevant experimental studies have been conducted to evaluate the flow attributes of liquid metals on the shell side of H-OTSG. Nevertheless, due to the similarity in structure, the flow of liquid metals in tube banks can be considered as a reference for such cases. The heat transfer characteristics of mercury over a staggered tube bank were investigated by Hoe et al. [11] and they concluded that the local heat transfer coefficient varies over the tube area, and it is higher in the front stagnation point than that of the rear stagnation point of the tubes. Kalish et al. [12] extensively studied the thermal behaviour of NaK in a 19-rod bundle structure, arranged in 90° crossflow and 45° oblique flows through the bundles. They found that the local heat transfer coefficient was lower for the 45° oblique layout, compared to the 90° arrangement. Chernysh et al. [13] determined the temperature and velocity profile of lead-based liquid metal flow over tube bundles and found that the presence of thermodynamically active oxygen reduces the heat transfer performance. Yang et al. [14] extensively studied the heat transfer properties of LBE in inclined tube bundles in low Peclet number (Pe) regions. They determined that the Nusselt number (Nu) of the inclined tube bundles is lower than the inline arrangement. Based on the experimental data, correlations for Nu of the inline and inclined tube bundles were formed.

Due to the challenges involved in conducting experimental studies on liquid metal flow, computational fluid dynamics (CFD) is instrumental in evaluating the flow attributes of liquid metals in tube banks. Abramov et al. [6] conducted a 2D, unsteady analysis of the temperature and velocity fields of liquid metal flow through smooth inline tube bundles and evaluated the influence of the domain size and Peclet number. They concluded that for both close-packed wide-placed tube bundle layouts, Nu increases with increment in Pe and the intensity of cross-flow in the intertubular spaces governs heat transfer. Even at moderate mesh, their developed model showed decent agreement with the experiment. Shen et al. [15] assessed the impact of helix angles on the thermal-hydraulic behaviour of LBE crossflow over helically coiled tube bundles. They found that due to the intensified turbulence intensity and generation of transverse flow, the highest Nu and friction factor (f) is achieved for a helix angle of 45° . The thermal behaviour of LBE in the inline and staggered arrangement was studied by Tassone et al. [16]. They concluded that the steady $k-\omega$ SST model combined with the varying turbulent Prandtl number model resulted in the most accurate numerical model. However, both steady-state and unsteady models predicted erroneous results for compact tube bundle layouts. Moreover, local heat transfer behaviour was not considered in this study. Xie et al. [17] used Direct Numerical Simulation (DNS) to examine the applicability of the Pr model and to assess the thermal performance of liquid metal in bare rod bundles, with varying Pr, Reynolds number (Re) and geometry parameters. From the numerical results, a correlation for Nu is derived. Jiang et al. [18] compared the thermal behaviour of water and mercury over staggered tube banks using the $k-\omega$ SST model combined with the Kays turbulent Pr model. They concluded that for mercury flow, molecular thermal diffusion is the largest contributor to heat transfer even in turbulent regimes, and the turbulent intensity is lower in the initial rows of the tube bundle than the later ones. They also noted that water resulted in a higher pressure drop than mercury. Yang et al. [19] derived correlations of Nu of LBE flow across inline and staggered layouts along with inclined tube bundles from numerical results. They found that both staggered and inclined layouts predicted lower Nu compared to inline tube bundles. However, the alternate inclination angle of the tubes significantly improved the heat transfer rate. Lee et al. [20] used Large Eddy Simulation (LES) to analyze the three-dimensional effects on the magnitude of velocity, pressure and vorticity in a five-layered helical coil tube bundle. They reported that the mean velocity in the w direction was generated due to the helical shape of the coils and it substantially complicated the flow structure. They also suggested a conservative design to withstand the long fluctuations in peak frequencies.

The concept of thermohydraulic enhancement in the flow of liquid metal on the shell side of H-OTSG is established, yet there remains a need for more comprehensive studies to fully grasp its implications. Further investigations are necessary to gain a nuanced understanding of the flow phenomena, improvements, and potential drawbacks. While most of the studies address LBE crossflow in tube banks, they do not accurately represent the more intricate shell-side flow in H-OTSG, which is inherently more complex. Therefore, unlike studies focused on the flow phenomenon above tube bundles, our research emphasizes thermal-hydraulic performance, an aspect that is still underexplored in the existing literature. Moreover, the limited literature available solidifies the concept, but it also raises questions about the optimization of designs, particularly regarding the tube arrangement, which is incremental to the thermal-hydraulic performance of a H-OTSG. Subsequently, this study seeks to address these gaps by assessing the influence of tube bank layout on the heat transfer and frictional behaviour of LBE crossflow. To determine the impact of tube bundle layout, various arrangements have been examined, including inline arrangement, obliquely staggered arrangement, triangular arrangement, and rotated square arrangement. To conduct the analysis, a numerical model has been developed and validated using experimental data and empirical correlations. The velocity field over the flow domain along with vortical structures, Nusselt number (Nu), friction factor

(f) and thermal enhancement factor (THEF) have been employed to assess and compare the performance deviation. The findings will advance the understanding of LBE behaviour in H-OTSG shells, aiding the nuclear energy community in designing compact heat exchangers for cooling in nuclear reactors.

2. Physical model & cases considered

The numerical study evaluates the heat transfer characteristics and flow patterns of lead-bismuth eutectic (LBE) in various layouts of tube bundles. The three-dimensional heat transfer model of the turbulent LBE flow in tube bundles was conducted using Ansys Fluent 2022 R1. The computational domain depicted in Fig. 1 has a height of 300 mm, is made up of 35 tubes with a diameter of 15 mm, and is organised into 7 rows of 5 tubes each, as prescribed by Yang et al., [14]. The positioning and arrangement of tubes significantly impact the flow and heat transfer characteristics during crossflow over tube bundles [17]. Therefore, the objective of this investigation is to observe the impact of inline and staggered layouts on the performance of LBE flow across tube banks. Hence, several layouts of the tube bundles are considered for this numerical investigation including inline tube bundles (case 1), tube bundles with separate oblique angles (case 2–4), triangularly staggered arrangement (case 5) and staggered layouts with square spacing (case 6–7) with different diagonal pitches (S_D). The flow regime is kept between Peclet number (Pe) of 90–340. To accurately measure the change in thermal and frictional behaviour the tube bundles were designed at a fixed longitudinal pitch (S_L) and transverse pitch (S_T) of 18 mm. The design specification of the investigated cases is exhibited in Table 1.

2.1. Governing equations

The following equations were used to model the three-dimensional incompressible flow LBE in tube banks.

Continuity Equation [17]:

$$\frac{\partial(\rho u_i)}{\partial x_i} = 0 \tag{1}$$

Momentum Equation [17]:

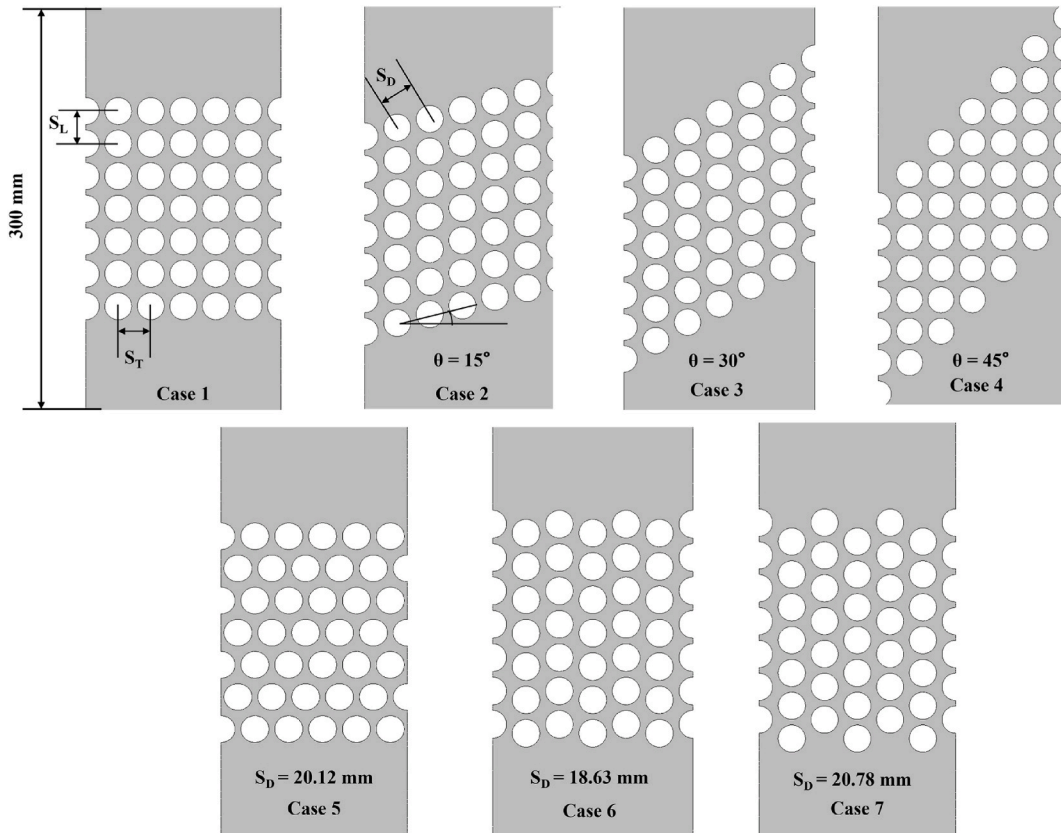


Fig. 1. Schematic representation of the tube bundle layout.

Table 1
Geometrical parameters of the cases considered.

Cases	S_T (mm)	S_L (mm)	S_D (mm)	θ (°)	Arrangement
1	18	18	25.46	–	In line
2	18	18	18.63	15	Staggered
3	18	18	20.78	30	Staggered
4	18	18	25.46	45	Staggered
5	18	18	20.12	–	Staggered
6	18	18	18.63	–	Staggered
7	18	18	20.78	–	Staggered

$$\frac{\partial(u_i u_j)}{\partial x_j} = \frac{1}{\rho} \frac{\partial p}{\partial x_i} + \frac{\partial}{\partial x_j} \left[(\nu + \nu_t) \left(\frac{\partial u_i}{\partial x_j} + \frac{\partial u_j}{\partial x_i} \right) \right] \quad (2)$$

Energy equation [17]:

$$\frac{\partial(u_j T)}{\partial x_j} = \frac{\partial}{\partial x_j} \left[\left(\frac{\nu}{Pr} + \frac{\nu_t}{Pr_t} \right) \frac{\partial T}{\partial x_j} \right] \quad (3)$$

here, the fluid density is denoted as ρ , the fluid velocity is u (ms^{-1}), p depicts the fluid pressure (Pa), the fluid temperature is represented as T (K), ν portrays the kinematic viscosity of the fluid, Pr defines the Prandtl number of the fluid which is the ratio of momentum diffusivity and thermal diffusivity [21], ν/Pr depicts the molecular thermal diffusivity and ν_t/Pr_t characterizes the turbulent thermal diffusivity.

To conduct the numerical analysis, the $k-\omega$ SST turbulence model is utilized due to its accurate performance in liquid metal flow over tube bundles [22]. In the SST $k-\omega$ turbulence model, k and ω depict the turbulent kinetic energy and diffusion of turbulent energy, respectively.

2.2. Modelling turbulent Prandtl number

Due to the Prandtl number of LBE being in the magnitude of 10^{-2} , the thermal dissipation process is mainly dominated by molecular conduction, even in fully turbulent regions [23]. Therefore, the heat transfer process of LBE is very different when compared to conventional fluids. Subsequently, the Reynolds analogy which considers $Pr_t \approx 1$ (turbulent Prandtl number), assuming similarity in the transport of heat and momentum is no longer valid for LBE flow. Hence, different turbulent Prandtl number model has been developed for modelling the flow of liquid metal over the years [23–27]. The model proposed by Kays has been utilized in this study as the model showed good performance in the bundle flow of heavy liquid metals [28].

The Kays turbulent Prandtl number model [24] is as follows,

$$Pr_t = 0.85 + \frac{0.7}{Pe_t} \quad (4)$$

where, Pe_t is the turbulent Peclet number which can be determined from:

$$Pe_t = \frac{\nu_t}{\nu} Pr \quad (5)$$

2.3. Mathematical formulations

Reynolds number (Re) can be formulated from the following equation [29]:

$$Re = \rho u_{max} d / \mu \quad (6)$$

here, ρ is the density (kg/m^3) of LBE, and the maximum velocity (ms^{-1}) of the tube bundle is denoted as u_{max} , d is the tube diameter (m) and μ is the dynamic viscosity (Pa s).

The Peclet number (Pe) of the tube bundle is defined as [18]:

$$Pe = C_p d \rho u_{max} / k \quad (7)$$

where the specific heat (J/kg.k) is represented by C_p , and the thermal conductivity (W/m.K) is depicted by k . u_{max} is the maximum velocity (ms^{-1}) across the tube bundle can be calculated from Ref. [29]:

$$u_{max} = u_{in} / \left(1 - \frac{d}{S_t} \right) \quad (8)$$

in which u_{in} represents the inlet velocity (ms^{-1}).

The pressure drop across the tube banks is calculated from the correlation of Zukauskas which is as follows [30]:

$$\Delta P = \left(\frac{\xi}{\chi}\right) \chi \frac{1}{2} \rho u_{max}^2 n \quad (9)$$

$$f = \left(\frac{\xi}{\chi}\right) \chi = \frac{2\Delta P}{\rho u_{max}^2 n} \quad (10)$$

in which ΔP is the pressure drop (Pa) across the tube bundle, ξ and χ are coefficients in the graphs, f is the friction factor and n is the number of tubes.

The Nusselt number (Nu) can be calculated from the given expression [31]:

$$Nu = hd/k \quad (11)$$

here, h is the heat transfer coefficient (W/m^2K), which can be calculated from the following equation [15]:

$$h = q^w / (T_{wall} - T_{avg}) \quad (12)$$

in which q^w is the heat flux (W/m^2) employed to the tubes, T_{wall} is the tube temperature (K) and T_{avg} is the average temperature of the fluid.

The average temperature of the fluid is evaluated from:

$$T_{avg} = \frac{T_{in} + T_{out}}{2} \quad (12)$$

here, T_{in} and T_{out} are the inlet and outlet temperature (K) respectively.

The thermal enhancement factor (THEF) is calculated from the following expression [32]:

$$THEF = \frac{Nu/Nu_{ref}}{\left(\frac{f}{f_{ref}}\right)^{1/3}} \quad (13)$$

where Nu_{ref} and f_{ref} are the Nu and f of the reference case. In this study, the inline arrangement of case 1 is considered as the reference.

The thermophysical properties of LBE are evaluated from the following equations provided by the Working Group on Lead-bismuth Eutectics from the Nuclear Energy Agency (NEA) [33].

The density of LBE is calculated from the following equation:

$$\rho = 11096 - 1.3236T \quad (14)$$

The specific heat capacity is evaluated from:

$$c_p = 159 - 2.72 \times 10^{-2}T + 7.12 \times 10^{-6}T^2 \quad (15)$$

The dynamic viscosity of LBE is calculated using the following expression:

$$\mu = 4.94 \times 10^{-4} \exp\left(\frac{754.1}{T}\right) \quad (16)$$

The thermal conductivity of LBE is obtained from the below equation:

$$k = 3.61 + 1.517 \times 10^{-2}T - 1.741 \times 10^{-6}T^2 \quad (17)$$

The thermo-physical properties of LBE are not kept constant due to the high-temperature gradient in the system. Instead, the property equations of LBE were modelled into user-defined functions (UDF) and they were incorporated into the Ansys Fluent console to account for the effect of temperature on the flow behaviour. It enables the incorporation of temperature-dependent variations in thermophysical properties within the numerical method [34,35].

2.4. Boundary conditions

In this investigation, the thermal and hydraulic performance of LBE in tube bundles is evaluated using Ansys Fluent. All the simulations were performed at Pe reaching 90–340. A uniform and constant velocity, with a homogenous temperature of 573K is prescribed at the flow domain inlet whereas the pressure outlet is considered for the exit region. The velocity direction at the inlet is in the positive y direction. The tube bundles were subjected to a constant heat flux of 20,000 W/m^2 to maintain thermal conditions akin to the experiment conducted by Ref. [16]. No-slip condition is applied to the walls, excluding the front and back walls where the symmetry boundary condition is proposed. The effect of turbulence is analyzed using the SST k- ω turbulence model. The employed boundary conditions of the current case study are exhibited in Fig. 2.

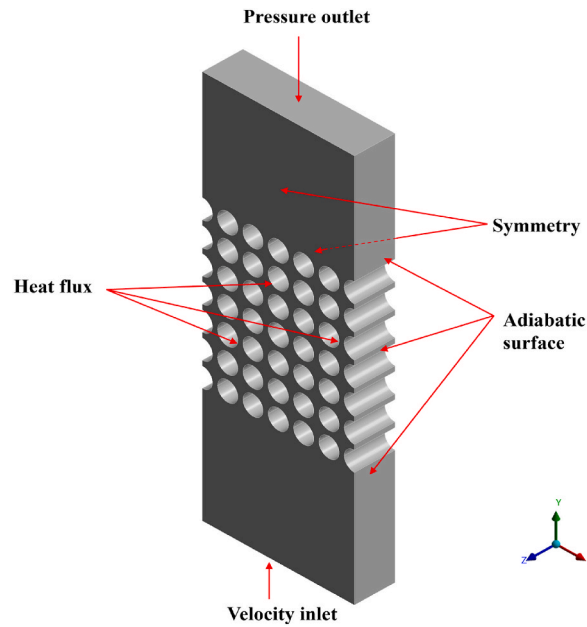


Fig. 2. Schematic representation of the computational domain and employed boundary conditions.

2.5. Numerical approach and grid sensitivity analysis

To reduce the number of generated elements and to increase the computation speed, poly-hex-core mesh has been used to discretize the computational domain. In this method, hexagonal cells are generated to fill the volume, whereas isotropic poly-prisms cells are generated in the boundary layer with the Mosaic polyhedral elements. Compared to conventional hex-core and tetrahedral elements, the poly-hex-core mesh has been reported to reduce the number of elements by 50%, while improving the computational speed by 20–50%, without any deviation in the results [36]. While creating the mesh, $y^+ < 1$ has been ensured to accurately capture the flow behaviour of LBE near the heater tube walls. The grid generation of the geometry is portrayed in Fig. 3.

This steady, three-dimensional simulation is solved using the finite volume-based solver of Ansys Fluent. For the coupling of pressure and velocity and the discretization of convection and diffusion terms, the SIMPLEC method is employed. This method, coupled with a second-order upwind scheme, is utilized for both momentum and energy equations. The convergence criterion is set to

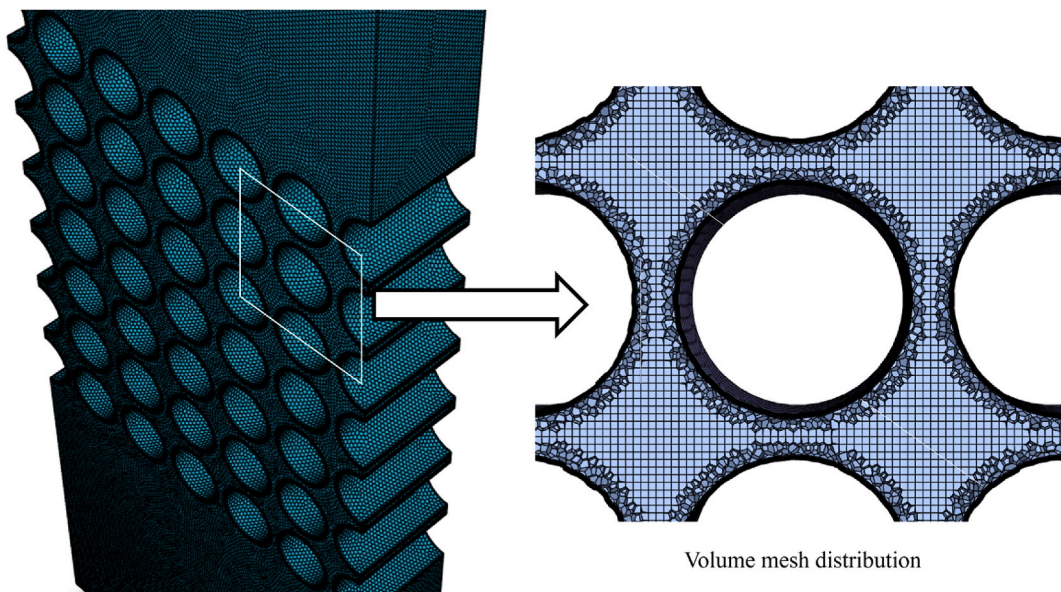


Fig. 3. Representation of the tube bundle mesh.

Table 2
Variation of Nusselt number and friction factor with grid sizes.

Serial no	Number of cells	Nu	% Diff Nu	f	% Diff f
1	675,889	8.13	6.39	0.507	5.35
2	1,422,925	7.61	2.10	0.479	4.75
3	2,134,388	7.45	0.67	0.457	0.21
4	3,415,020	7.41	–	0.453	–

be 10^{-4} for momentum and continuity and 10^{-6} for energy, attributed to the higher thermal diffusivity of LBE.

A mesh sensitivity analysis has been conducted with four different grid numbers as shown in Table 2. In order to perform the sensitivity analysis, simulations were conducted for the inline layout at a Peclet number of 340. Inspecting the deviations in the numerical results portrays that the difference between the numerically obtained Nu and f for cell numbers 2,134,388 and 3,415,020 is less than 1%. This implies that, with the extended simulation time, the results exhibited minimal deviation even with a more refined mesh. Therefore, a cell number of 2,134,388 is determined chosen for this investigation.

2.6. Model validation

To ensure the accuracy of the current numerical model, the results of the current simulation have been compared with experimental data and correlation. Nu at Pe of 90–350 has been validated by contrasting them with the experimental data of Yang et al. [14] as depicted in Fig. 4(a), while Fig. 4(b) shows f obtained from the current numerical model and Zukauskas correlation (Eq. (10)) at a similar range of Peclet number. The geometry used in the experimental study consists of 35 tubes, arranged in 7 rows and 5 columns. The diameter of the tube is 15 mm, and the pitch-to-diameter ratio is 18 mm. At the inlet of the domain, uniform velocity and temperature of LBE are prescribed. A uniform heat flux of $20,000 \text{ w/m}^2$ is applied to the tube surfaces, to maintain thermal conditions akin to the experiment conducted by Ref. [14]. As depicted in the figures, a reasonable agreement is exhibited between the numerical results and experimental data for the Nu, the maximum difference being less than 10%. For f . The maximum deviation between the computational model and the Zukauskas correlation is less than 7%. Therefore, with the implementation of the SST $k-\omega$ turbulence model along with the Kays turbulent Prandtl number model, precise prediction of the variation of Nu and f at different Pe is observed.

3. Results & discussion

In this numerical investigation, a 3D, steady heat transfer model of LBE crossflow in tube bundles is analyzed using Ansys Fluent. The influence of tube bundle layouts on the thermo-hydraulic performance is calculated for seven different cases by evaluating the velocity distribution, turbulence intensity, Q criterion, Nu and ff, at the flow range of $90 \leq \text{Pe} \leq 340$.

3.1. Effect of tube bundle layout on the flow pattern of LBE

The velocity fields of the tube bundles are illustrated in Fig. 5, which depicts the deviation in velocity magnitude influenced by the variation of the tube bundle layout. The velocity field of the inline arrangement (case 1) shows a strong presence of parallel flow and a higher velocity is observed between adjacent tubes. However, a significant amount of crossflow is also induced in case 1, which causes the asymmetrical low-velocity vortices to form downstream of the tubes. Depending on the volume of transverse flow, the generated

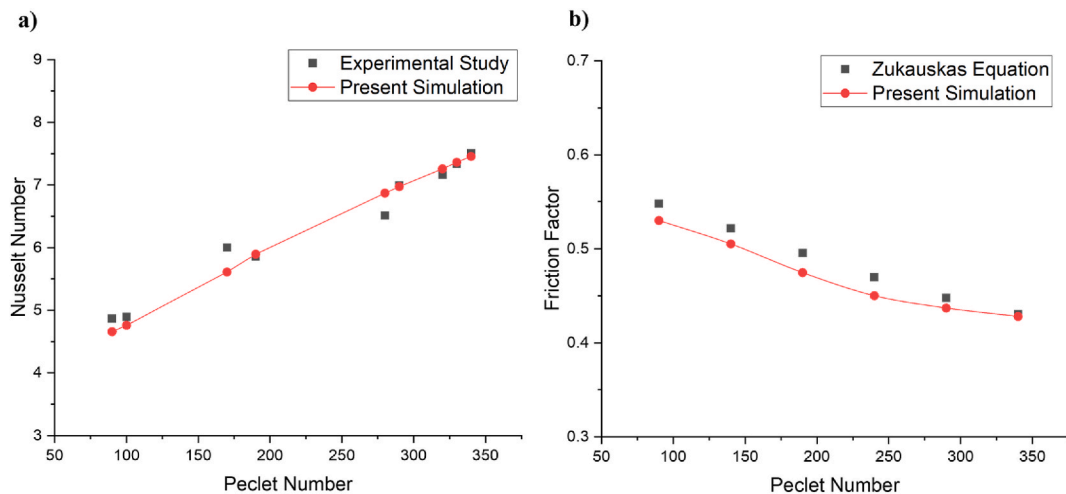


Fig. 4. a) Validation of Nu with the experimental results of Yang et al. [14] and b) validation of f with the correlation of Zukauskas [30].

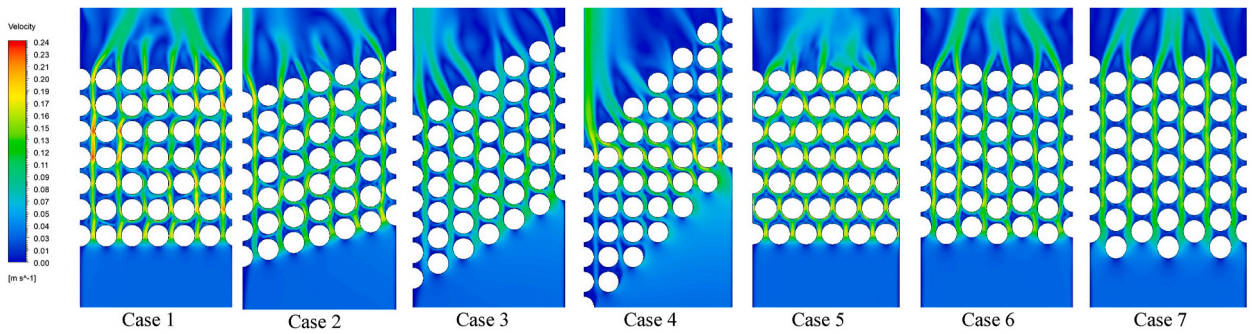


Fig. 5. The velocity distribution of the flow domain across inline and staggered tube bundle layouts, at a Peclet number of 340.

vortices shrink and shift towards either side of the tube. The presence of substantial crossflow enhances the fluid mixing in the tube bundles, augmenting Nu and f of Case 1. Increasing the oblique angle decreases the average velocity magnitude inside the channel as portrayed in the contours of case 2–4. However, it has a diverse impact on the overall flow structure and development of crossflow in the tube bundles. For case 2, the flow is evenly distributed throughout the channel, and the flow structure resembles that of case 1, albeit with a lower velocity. In the central columns, downstream of the tubes, the developed low-speed region is not prominent due to the high amount of mixing. In contrast, adjacent to the wall the vortices formed are more significant, which reduces Nu and f . For case 3, a lower amount of fluid mixing happens as crossflow occurrence is reduced and the velocity magnitude behind the tubes gets subdued. Compared to the other layouts, case 4 illustrates a unique flow structure. Parallel flow predominates in the regions near the side wall of the channel; however, in the central region, cross flow prevails over parallel flow and enhanced turbulent mixing occurs. In the vicinity of the leftmost tube bundle, the velocity magnitude is at its minimum, and the wake zone increases, exhibiting a significant reduction in the velocity of the generated vortices. Near the rightmost tube bundle, flow speed is augmented, and the produced vortices are less prominent as they are influenced by crossflow between the tubes.

As alternative positioning of tubes in adjacent rows creates frequent disturbances, crosswise flow transpires more swiftly in case 5, inducing strong turbulent mixing. The velocity field exhibits a greater level of uniformity in comparison to other cases, and higher flow speed occurs between adjacent tubes. Symmetrical vortices arise downstream of the tubes. Compared to case 1, case 5 illustrates a more stable and uniform transverse flow. Due to enhanced flow mixing and occurrence of crossflow, both Nu and f increase for case 5. Both case 6 and case 7 are dominated by parallel flow, giving rise to large wake zones behind the tubes. The predominant parallel flow decreases the Nu for these cases.

As the flow of LBE in tube bundles induces notable wake and swirl regions, the potential for creating hotspots and variations in local oxygen concentration becomes apparent, as mentioned in previous investigations [37]. This can lead to significant corrosion in the reactor wall and degradation in the coolant properties [38]. Therefore, when designing such devices, enough fluid mixing is crucial to avoid the creation of high-temperature regions and in this context, case 5 stands out as particularly beneficial, as it demonstrates enhanced fluid mixing. However, the corrosion of the reactor wall also depends on the material being used, and ceramics such as Aluminum Nitride (AlN) is showing amazing prospect due to their exceptional corrosion resistance in harsh conditions and high thermal conductivity [39].

3.2. Impact of tube bundle arrangement on the vortical structures

Q criterion, which is a scalar quantity indicates the presence of vortical structures in the flow domain. Positive values of this criteria portray regions with vortices or swirling motion, while negative Q values indicate areas with shear flow. To examine the influence of different tube bundle layouts on vortex structures, the distribution of the Q criterion has been assessed, as illustrated in Fig. 6. Here, the

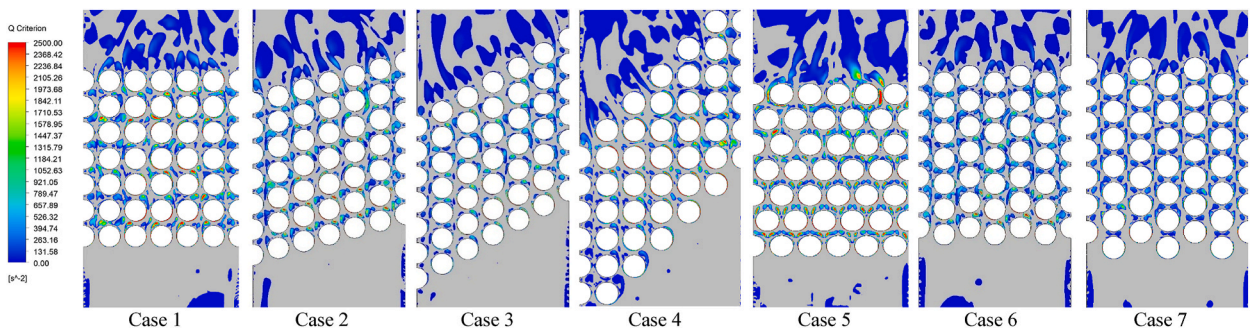


Fig. 6. The vortical structures across the inline and staggered layouts of the tube bundle, at a Peclet number of 340.

Q criterion is considered for values greater than zero ($Q > 0$) and negative values are excluded from the analysis.

For case 1 and case 5, the enhanced magnitude of the Q criterion is observed, which indicates that for these cases, stable vortices with high intensity are formed, ensuring substantial cross-flow and turbulent mixing. The intensification of the Q criterion of case 1 and case 5 confirms the improvement of heat and momentum transfer. For case 5, two different types of vortex structures are observed, a weakened region with symmetrical vortices downstream of the tubes, and an intensified and stable vortex region beside the weakened vortices. Further downstream, the symmetrical vortex structures are broken down and strengthened, giving rise to more amplification of fluid mixing. The vortex structures of case 1 are randomly distributed an enhanced Q value is examined behind the tube bundles. Compared to other cases, case 5 depicted considerably stronger vortex structures.

The inclusion of oblique angle changes the vortex region in the tube bundles. Steady vortices are observed for case 2, however case 3 shows subdued vortices. Hence, fluid mixing is substantially diminished in case 3 as the generated vortices are not prominent enough to induce crossflow. For case 4, enhanced vortexes are formed at the rightmost boundary region, while weak vortices occur at the leftmost area. Therefore, a higher amount of mixing and transverse flow transpires in the rightmost region for case 4. Moderate swirling motion is observed behind the tubes for case 6, however, weaker vortices dominate the bundle region for case 7, significantly decreasing the magnitude of turbulent mixing.

3.3. Influence of tube bundle layout on turbulence intensity

Turbulent intensity is an essential criterion to determine the performance of LBE in cross-flow, as it indicates the rate or degree of turbulence present in the flow domain. A higher value of turbulence intensity ensures a high quantity of fluid mixing and enhanced heat transfer performance.

The turbulence intensity distribution across the tube banks is portrayed in Fig. 7. High turbulence intensity is observed both downstream of the tubes and in the longitudinal flow direction for case 1, confirming enhanced intermixing of fluids and amplified heat transfer rate. Similarly, a high rate of uniformly distributed turbulence mixing occurs in case 5 and the flow domain increased turbulence intensity all over the flow domain. The inclusion of an oblique angle reduces the magnitude of turbulence intensity in the flow domain as seen in case 2 and case 3. When the oblique angle is $0^\circ < \theta < 45^\circ$, intensified turbulence is observed at the wake region of the tubes, and lower intensity is seen in the longitudinal flow direction. When θ is 45° , increased turbulence intensity is observed at the centre region of the tube bundles. However, areas near the boundary show reduced intensity. As parallel flow dominates the flow field of case 6 and case 7 and cross-flow gets diminished, the turbulence intensity becomes considerably lower and the heat transfer performance is reduced.

3.4. Deviation in heat transfer rate and pressure drop performance

The average Nu, f and thermal enhancement factor (THEF) at different Peclet numbers have been evaluated and illustrated in Figs. 8–10, respectively. As depicted in Fig. 8, case 5 shows the highest magnitude of Nu, followed by the inline configuration of Case 1, which showed substantial transverse flow in the flow field. However, the frequent disturbance caused by the tube arrangement of case 5 induced even stronger crossflow in the flow domain, resulting in enhanced flow mixing and heat transfer. As a result, compared to case 1, the Nu of case 5 increases considerably, along with its f as presented in Fig. 9. As the oblique angles increased, the f showed a gradual decrease. Additionally, in case 2 and case 3, the Nu also exhibited a decline with higher oblique angles. This can be attributed to the significant diminution of crosswise flow, leading to much lower turbulence in the flow domain. In contrast, at an oblique angle of 45° , the centre rows of case 4 exhibit the tube layout of inline arrangement. This configuration induces heightened transverse flow in the central region, overpowering parallel flow. Therefore, the Nu of case 4 is of a higher magnitude than case 3. Increasing the diagonal spacing also intensifies the dominance of parallel flow and increases the wake region in case 6 and case 7. Subsequently, the Nu sharply declined for both cases. Nonetheless, increasing the diagonal distance of cases 6 and 7 caused frequent disturbances in the parallel flow direction, increasing the pressure drop. However, these disturbances are not enough to induce crossflow. Hence, the f of case 6 is greater than cases 2–4 but lower than case 1. At an increased diagonal distance, case 7 resulted in a higher pressure drop and the friction factor exhibited a slightly higher value than in case 1. For all the cases, Nu increases with the Pe while the f decreases.

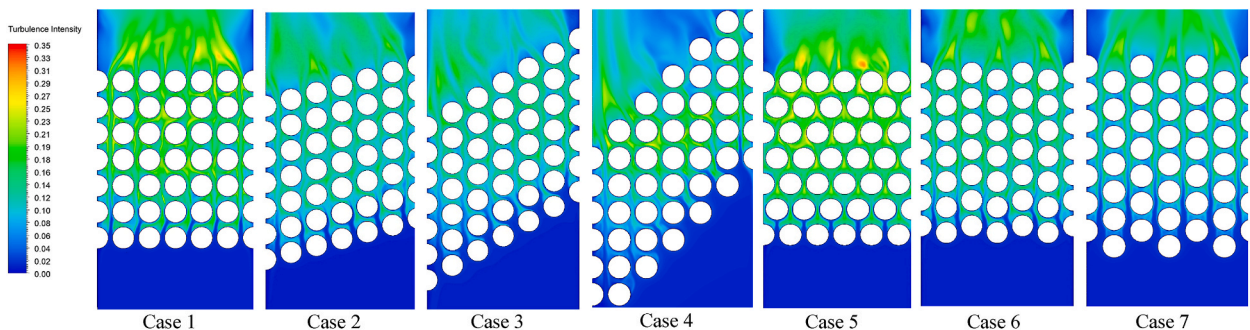


Fig. 7. Influence of inline and staggered tube bundle arrangements on turbulence intensity, at a Peclet number of 340.

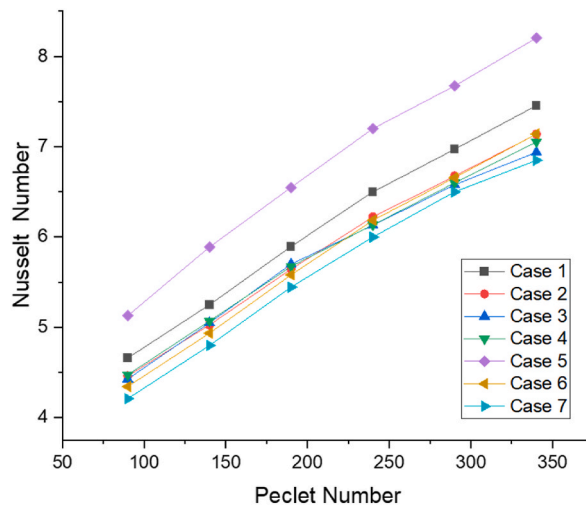


Fig. 8. Variation of Nusselt number of LBE at different Peclet numbers and tube bundle layout.

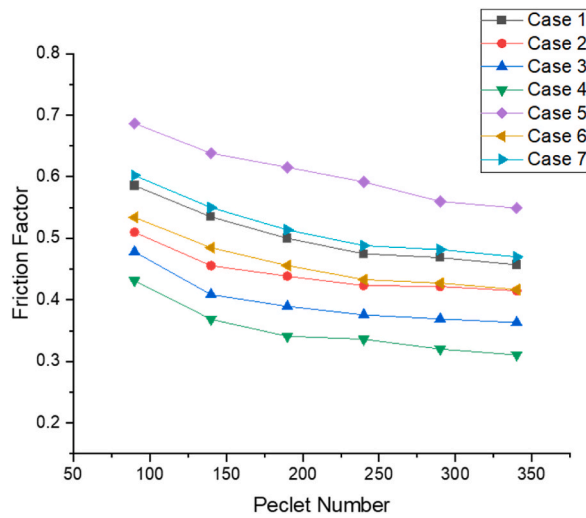


Fig. 9. Change in friction factor of LBE with respect to Peclet number for the investigated cases.

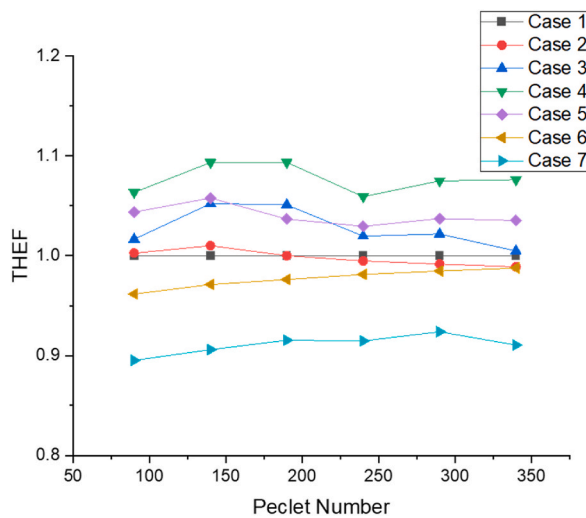


Fig. 10. Influence of tube bank layout on the THEF of LBE crossflow, at varying Peclet numbers.

The THEF value depends on Nu and f across the flow domain. It indicates the improvement of thermal performance by comparing it to a reference case, where a magnitude higher than unity indicates enhanced thermal effectiveness. Fig. 10 represents the THEF value of the cases at different Peclet numbers. In this investigation, the inline arrangement of case 1 is considered as a reference. As illustrated in Fig. 10, only case 3, case 4, and case 5 exhibited an enhancement in THEF across the entire range of Peclet numbers, case 4 being the highest, followed by case 5 and case 3. Case 6 and case 7 showed diminished thermal performance throughout the entire range of Peclet numbers. For case 2, the THEF value is slightly greater than unity at lower Peclet numbers, but it decreases at higher Peclet numbers.

4. Conclusion

In this study, the influence of tube bank arrangement in the crossflow of LBE is investigated. The thermal and frictional characteristics of LBE crossflow have been evaluated for inline, obliquely staggered, triangular and rotated square arrangements. The SST $k-\omega$ turbulence model combined with the Prandtl number model of Kays are used in this numerical model, and the results of the simulation have been validated against experimental data and correlations. The main findings of this investigation are drawn below:

- The inline and triangular arrangement of tube banks shows a substantial magnitude of crossflow, enhancing flow mixing. Increasing the oblique angles reduces the occurrence of crosswise flow, reducing turbulent mixing. However, for an oblique angle of 45° , the central region assumes the layout of inline arrangement, which increases transverse flow. Parallel flow dominates in the case of rotated square arrangements.
- Due to significant crossflow in the flow domain, the triangular tube arrangement depicts considerable turbulence, followed by the inline arrangement. The induced turbulence plummets for rotated square and oblique arrangements.
- The triangular arrangement of the tubes depicted a considerably higher Nu of 8.2 and f of 0.55 at Pe of 340, which is around 10% and 20 % higher than the Nu and f of the inline arrangement, respectively. In Case 1, the inline arrangement demonstrates a Nu of 7.45, accompanied by a f of 0.45. However, the induced crossflow in the central region resulted in a Nu of 7.05 when the oblique angle was 45° . This value is 5% less than the inline arrangement but greater than Case 3 with an oblique angle of 45° , which is approximately 8% less than the inline arrangement due to diminished turbulence. Nu also drops for the rotated square layout, while the f depicts a slight enhancement of 4% than the inline arrangement at a higher diagonal pitch.
- The triangular layout and oblique layout with 30° and 45° angles showed maximum thermal effectiveness of 1.06, 1.1 and 1.05, respectively, when the inline arrangement is considered as the reference. For all the other cases, the magnitude of THEF is under unity, being 0.98, 0.96 and 0.89 for case 2, case 6 and case 7 respectively.

The current investigation only focuses on the shell side flow of LBE and the impact of tube bundles on the thermal-hydraulic performance. However, the tube flow is not considered to simplify the computational process. In the future, comprehensive investigations should extend beyond the LBE flow on the shell side. The optimization of flow conditions on the tube side and the selection of an optimal working fluid deserve attention. Moreover, to enhance the applicability of the findings to practical applications, numerical investigations should be complemented by rigorous experimental studies.

Additional information

No additional information is available for this paper.

CRedit authorship contribution statement

Mashrur Muntasir Nuhash: Writing – original draft, Visualization, Validation, Software, Methodology, Investigation, Formal analysis, Data curation, Conceptualization. **Md. Rezwanul Karim:** Writing – review & editing, Supervision, Resources, Project administration, Funding acquisition. **Arafat A. Bhuiyan:** Writing – review & editing, Supervision, Investigation, Conceptualization.

Declaration of competing interest

The authors declare that they have no known competing financial interests or personal relationships that could have appeared to influence the work reported in this paper.

Nomenclature

C_p	specific heat (J/kg.K)
d	tube diameter (m)
f	friction factor
h	convective heat transfer coefficient ($W/m^2 \cdot K$)
k	thermal conductivity ($W/m.K$)
Nu	Nusselt number
n	number of tubes

Pe	Peclet number
Pe _t	turbulent Peclet number
Pr	Prandtl number
Pr _t	turbulent Prandtl number
ΔP	pressure drop (N/m ²)
S _D	diagonal pitch (mm)
S _L	longitudinal pitch (mm)
S _T	transverse pitch (mm)
q ^w	heat flux on the tube wall (W/m ²)
Re	Reynolds number
T	temperature (K)
u _{in}	inlet velocity (m/s)
u _{max}	maximum velocity (m/s)

Abbreviations

CFD	computational fluid dynamics
LBE	lead-bismuth eutectic
THEF	thermal enhancement factor

Greek letters

ξ	coefficient related to pressure drop
χ	coefficient related to pressure drop
θ	oblique angle (°)
μ	dynamic viscosity (mPa.s)
ρ	density (kg/m ³)
ν	kinematic viscosity (m ² /s)

Subscripts

avg	average
in	inlet
out	outlet
ref	reference
max	maximum

References

- [1] A. Abbas, M. Ashraf, H. Ahmad, K. Ghachem, Z. Ullah, A. Hussanan, T. Labidi, L. Kolsi, Computational analysis of Darcy-Forchheimer relation, reduced gravity, and external applied magnetic field influence on radiative fluid flow and heat transfer past a sphere: finite difference method, *Heliyon* 9 (2023), <https://doi.org/10.1016/j.heliyon.2023.e15696>.
- [2] A. Abbas, I.E. Sarris, M. Ashraf, K. Ghachem, N. Hnaïen, B.M. Alshammari, The effects of reduced gravity and radiative heat transfer on the magnetohydrodynamic flow past a non-rotating stationary sphere surrounded by a porous medium, *Symmetry (Basel)* 15 (2023), <https://doi.org/10.3390/sym15040806>.
- [3] F.G. Agayev, S.V. Trukhanov, A.V. Trukhanov, S.H. Jabarov, G.S. Ayyubova, M.N. Mirzayev, E.L. Trukhanova, D.A. Vinnik, A.L. Kozlovskiy, M.V. Zdorovets, A.S. B. Sombra, D. Zhou, R.B. Jotania, C. Singh, A.V. Trukhanov, Study of structural features and thermal properties of barium hexaferrite upon indium doping, *J. Therm. Anal. Calorim.* 147 (2022) 14107–14114, <https://doi.org/10.1007/s10973-022-11742-5>.
- [4] Y. Zhang, C. Wang, Z. Lan, S. Wei, R. Chen, W. Tian, G. Su, Review of thermal-hydraulic issues and studies of lead-based fast reactors, *Renew. Sustain. Energy Rev.* 120 (2020), <https://doi.org/10.1016/j.rser.2019.109625>.
- [5] J.E. Kelly, Generation IV International Forum: a decade of progress through international cooperation, *Prog. Nucl. Energy* 77 (2014) 240–246, <https://doi.org/10.1016/j.pnucene.2014.02.010>.
- [6] A.G. Abramov, A.M. Levchenya, E.M. Smirnov, P.E. Smirnov, Numerical simulation of liquid metal turbulent heat transfer from an inline tube bundle in cross-flow, *St. Petersburg Polytechnical Univ. J.: Phys. Mathemat.* 1 (2015) 356–363, <https://doi.org/10.1016/j.spjpm.2016.02.002>.
- [7] M. Caramello, C. Bertani, M. De Salve, B. Panella, Helical coil thermal-hydraulic model for supercritical lead cooled fast reactor steam generators, *Appl. Therm. Eng.* 101 (2016) 693–698, <https://doi.org/10.1016/j.applthermaleng.2016.01.028>.
- [8] A. Abbas, R. Khandelwal, H. Ahmad, A. Ilyas, L. Ali, K. Ghachem, W. Hassen, L. Kolsi, Magnetohydrodynamic bioconvective flow of williamson nanofluid over a moving inclined plate embedded in a porous medium, *Mathematics* 11 (2023), <https://doi.org/10.3390/math11041043>.
- [9] F. Chen, X. Huai, J. Cai, X. Li, R. Meng, Investigation of turbulent-Prandtl-number models for liquid lead-bismuth eutectic, *Nucl. Eng. Des.* 257 (2013) 128–133, <https://doi.org/10.1016/j.nucengdes.2013.01.005>.
- [10] A. Shams, A. De Santis, F. Roelofs, An overview of the AHFM-NRG formulations for the accurate prediction of turbulent flow and heat transfer in low-Prandtl number flows, *Nucl. Eng. Des.* 355 (2019), <https://doi.org/10.1016/j.nucengdes.2019.110342>.
- [11] R.J. Hoe, D. Dropkin, O.E. Dwyer, Heat-transfer rates to crossflowing mercury in a staggered tube bank—I, *J. Fluid Eng.* 79 (1957) 899–905, <https://doi.org/10.1115/1.4013177>.
- [12] S. Kalish, O.E. Dwyer, Heat transfer to NaK flowing through un baffled rod bundles, *Int. J. Heat Mass Tran.* 10 (1967) 1533–1558.
- [13] A. Chernysh, M. Iarmonov, K. Makhov, A. Beznosov, Experimental study of the characteristics of heat transfer in an HLMC cross-flow around tubes, *J. Nucl. Eng. Radiat. Sci.* 1 (2015), <https://doi.org/10.1115/1.4030365>.

- [14] Y. Yang, C. Wang, D. Zhang, S. Qiu, G. Su, W. Tian, Heat transfer evaluation of liquid lead-bismuth eutectic cross flow tube bundle: experimental part, *Int. J. Therm. Sci.* 193 (2023) 108527, <https://doi.org/10.1016/j.ijthermalsci.2023.108527>.
- [15] C. Shen, L. Liu, Z. Xu, H. Gu, M. Liu, Influence of helix angle on flow and heat transfer characteristics of lead–bismuth flow in helical-coiled tube bundles, *Ann. Nucl. Energy* 180 (2023) 109483, <https://doi.org/10.1016/j.anucene.2022.109483>.
- [16] A. Tassone, J. Meeusen, A. Serafini, G. Caruso, Numerical study of liquid metal turbulent heat transfer in cross-flow tube banks, *Energies* 16 (2023), <https://doi.org/10.3390/en16010387>.
- [17] X. Xie, H. Zhao, X. Li, X. Wu, F. Niu, Numerical investigation on heat transfer characteristics of liquid metal cross flow over tube bundles, *Ann. Nucl. Energy* 180 (2023), <https://doi.org/10.1016/j.anucene.2022.109465>.
- [18] H. Jiang, X. Wang, Y. Liu, Numerical study of different Pr number medium turbulent cross flow in staggered tube bundle, *Int. J. Therm. Sci.* 187 (2023), <https://doi.org/10.1016/j.ijthermalsci.2023.108206>.
- [19] Y. Yang, C. Wang, D. Zhang, S. Qiu, G. Su, W. Tian, Heat transfer evaluation of liquid lead-bismuth eutectic cross flow tube bundle: numerical simulation part, *Int. Commun. Heat Mass Tran.* 146 (2023) 106892, <https://doi.org/10.1016/j.icheatmasstransfer.2023.106892>.
- [20] S.J. Lee, Y.A. Hassan, Numerical investigation of helical coil tube bundle in turbulent cross flow using large eddy simulation, *Int. J. Heat Fluid Flow* 82 (2020) 108529, <https://doi.org/10.1016/j.ijheatfluidflow.2019.108529>.
- [21] A.M. Obalalu, T. Oreyeni, A. Abbas, M.A. Memon, U. Khan, E.S.M. Sherif, A.M. Hassan, I. Pop, Implication of electromagnetohydrodynamic and heat transfer analysis in nanomaterial flow over a stretched surface: applications in solar energy, *Case Stud. Therm. Eng.* 49 (2023), <https://doi.org/10.1016/j.csite.2023.103381>.
- [22] C. Wang, C. Wang, Y. Zhang, D. Zhang, W. Tian, G. Su, S. Qiu, Flow and heat transfer evaluation of lead-bismuth eutectic coolant for nuclear power application, *Nucl. Eng. Des.* 385 (2021), <https://doi.org/10.1016/j.nucengdes.2021.111550>.
- [23] X. Cheng, N. Il Tak, Investigation on turbulent heat transfer to lead-bismuth eutectic flows in circular tubes for nuclear applications, *Nucl. Eng. Des.* 236 (2006) 385–393, <https://doi.org/10.1016/j.nucengdes.2005.09.006>.
- [24] W.M. Kays, Turbulent Prandtl Number-Where Are We?. <http://heattransfer.asmedigitalcollection.asme.org/>, 1994.
- [25] B. Weigand, J.R. Ferguson, M.E. Crawford, An Extended Kays and Crawford Turbulent Prandtl Number Model, 1997.
- [26] M. Jischa, H.B. Rieke, About the Prediction of Turbulent Prandtl and Schmidt Numbers from Modeled Transport Equations, n.d..
- [27] A.J. Reynolds, The prediction of turbulent Prandtl and Schmidt numbers, *Int. J. Heat Mass Tran.* 18 (1975) 1055–1069.
- [28] Z. Ge, J. Liu, P. Zhao, X. Nie, M. Ye, Investigation on the applicability of turbulent-Prandtl-number models in bare rod bundles for heavy liquid metals, *Nucl. Eng. Des.* 314 (2017) 198–206, <https://doi.org/10.1016/j.nucengdes.2017.01.032>.
- [29] M. Yu, G. Jiang, Y. Jiang, Y. Liu, W. Zhang, J. Sun, Experimental and numerical study of convective heat transfer in-line tube bundle by acoustic action, *Case Stud. Therm. Eng.* 44 (2023), <https://doi.org/10.1016/j.csite.2023.102869>.
- [30] A. Zukauskas, Heat transfer from tubes in crossflow, *Adv. Heat Tran.* (1972) 93–160.
- [31] O.E. Akay, M. Das, Modeling the total heat transfer coefficient of a nuclear research reactor cooling system by different methods, *Case Stud. Therm. Eng.* 25 (2021), <https://doi.org/10.1016/j.csite.2021.100914>.
- [32] A.L. Antony, S.P. Shetty, N. Madhwesh, N. Yagnesh Sharma, K. Vasudeva Karanth, Influence of stepped cylindrical turbulence generators on the thermal enhancement factor of a flat plate solar air heater, *Sol. Energy* 198 (2020) 295–310, <https://doi.org/10.1016/j.solener.2020.01.065>.
- [33] Handbook on Lead-bismuth Eutectic Alloy and Lead Properties, Materials Compatibility, Thermal-hydraulics and Technologies. www.oecd.org/publishing/corrigenda, 2015.
- [34] Z. Ullah, A. Hussain, M.S. Aldhabani, N.H. Altaweel, S. Shahab, Significance of temperature-dependent density on dissipative and reactive flows of nanofluid along magnetically driven sheet and applications in machining and lubrications, *Lubricants* 11 (2023) 410, <https://doi.org/10.3390/lubricants11090410>.
- [35] A. Abbas, A. Noreen, M. Ashraf Ali, M. Ashraf, E. Alzahrani, R. Marzouki, M. Goodarzi, Solar radiation over a roof in the presence of temperature-dependent thermal conductivity of a Casson flow for energy saving in buildings, *Sustain. Energy Technol. Assessments* 53 (2022) 102606, <https://doi.org/10.1016/J.SETA.2022.102606>.
- [36] K. Zore, B. Sasanapuri, G. Parkhi, A. Varghese, Ansys mosaic poly-hexcore mesh for high-lift aircraft configuration, in: *21th Annual CFD Symposium*, 2019.
- [37] A. Marino, J. Lim, S. Keijers, J. Deconinck, A. Aerts, Numerical modeling of oxygen mass transfer in a wire wrapped fuel assembly under flowing lead bismuth eutectic, *J. Nucl. Mater.* 506 (2018) 53–62, <https://doi.org/10.1016/j.jnucmat.2017.12.017>.
- [38] F. Roelofs, *Thermal Hydraulics Aspects of Liquid Metal Cooled Nuclear Reactors*, 2019.
- [39] A. Kozlovskiy, I. Kenzhina, Z.A. Alyamova, M. Zdorovets, Optical and structural properties of AlN ceramics irradiated with heavy ions, *Opt. Mater.* 91 (2019) 130–137, <https://doi.org/10.1016/j.optmat.2019.03.014>.